Soft Matter

PAPER

View Article Online
View Journal | View Issue

Cite this: *Soft Matter*, 2014, **10**, 590

Intermolecular forces between low generation PAMAM dendrimer condensed DNA helices: role of cation architecture

Min An, Sean R. Parkin and Jason E. DeRouchey*

Received 2nd August 2013
Accepted 4th November 2013

DOI: 10.1039/c3sm52096j

www.rsc.org/softmatter

In recent years, dendriplexes, complexes of cationic dendrimers with DNA, have become attractive DNA delivery vehicles due to their well-defined chemistries. To better understand the nature of the forces condensing dendriplexes, we studied low generation poly(amidoamine) (PAMAM) dendrimer–DNA complexes and compared them to comparably charged linear arginine peptides. Using osmotic stress coupled with X-ray scattering, we have investigated the effect of molecular chain architecture on DNA–DNA intermolecular forces that determine the net attraction and equilibrium interhelical distance within these polycation condensed DNA arrays. In order to compact DNA, linear cations are believed to bind in DNA grooves and to interact with the phosphate backbone of apposing helices. We have previously shown a length dependent attraction resulting in higher packaging densities with increasing charge for linear cations. Hyperbranched polycations, such as polycationic dendrimers, presumably would not be able to bind to DNA and correlate their charges in the same manner as linear cations. We show that attractive and repulsive force amplitudes in PAMAM–DNA assemblies display significantly different trends than comparably charged linear arginines resulting in lower DNA packaging densities with increasing PAMAM generation. The salt and pH dependencies of packaging in PAMAM dendrimer–DNA and linear arginine–DNA complexes were also investigated. Significant differences in the force curve behaviour and salt and pH sensitivities suggest that different binding modes may be present in DNA condensed by dendrimers when compared to linear polycations.

Introduction

Cationic dendrimers have shown potential as gene delivery vectors due to their ability to condense DNA and protect it from cellular and restriction nucleases.[1–4] Dendrimers are hyperbranched macromolecules with precisely defined molecular weights and highly symmetric branches stemming from a central core. Each generation of dendrimer represents an iterative growth step resulting in twice the number of reactive surface groups of the preceding generation. Due to their potential as gene delivery agents, characterization of packaging and forces within cationic dendrimer–DNA complexes, or dendriplexes, is needed. Theoretical studies and simulations have predicted behaviour similar to a semi-flexible polyelectrolyte interacting with a hard sphere with wrapping of DNA around dendrimers or so-called "beads on a string" structures possible.[5,6] However, early experimental studies have shown highly varied results with relation to the structure inside the dendriplexes. Depending on the dendrimer chemistry and generation, tetragonally and hexagonally packaged columnar mesophases, as well as DNA wrapping, have been reported in dendrimer–DNA complexes as observed by small angle X-ray scattering (SAXS), atomic force and transmission electron microscopy (AFM and TEM) experiments and single molecule tweezing.[7–17] While large generation dendrimers are thought to have spherical shapes, low generation dendrimers are estimated to be more disc-like.[18] In this study, we focus on low generation poly(amidoamine) (PAMAM) dendrimers.

The physical origins of the forces acting on DNA condensation are still debated. Experimental studies have aimed to elucidate the fundamental physical mechanisms responsible for DNA condensation.[19–28] *In vitro* experiments have shown that DNA condensation from bulk solution critically depends on the cation net charge. Typically +3 or larger cations are required to overcome the inherently large electrostatic repulsive barrier between the like-charged double stranded DNA.[29,30] Upon condensation, the resulting compacted structures have well defined equilibrium surface separations. Depending on the identity of the cation, these surface separations between DNA helices range from 7–15 Å. The finite separation of helices indicates a delicate balancing of a short range repulsive force with a longer range attraction.[19,24,25] Concurrent to experiments, theoretical studies have also been pursued to shed light on the nature of these condensed soft matter phases. This work is driven in part by the inability of the classical Poisson–Boltzmann (PB) mean-field theory to fully

Department of Chemistry, University of Kentucky, Lexington, Kentucky 40506, USA. E-mail: derouchey@uky.edu; Fax: +1 859 323 1069; Tel: +1 859 323 2827

explain the observed attractions in DNA condensation.[31] Theoretical treatments of the interhelical forces range from classical electrostatics in a continuum dielectric[32–34] to hydration interactions that emphasize the disruption of water structures in tight spaces.[19,24,35] To account for the attractions driving DNA condensation, these theories require correlations of charges or water structuring. A recently proposed electrostatic zipper model by Kornyshev and Leikin provides a convenient model for discussing correlations and attractions.[36–38] They propose binding of cationic charges in the major or the minor grooves, thus leading to attractive interhelical correlations between the bound positive charges and the phosphate backbone of apposing helices. Experimental studies suggest that such groove binding is present in a variety of linear polycations.[39–43] Hyperbranched polycations, such as polycationic dendrimers, presumably would not be able to bind to DNA and correlate their charges with the phosphates of adjoining DNA in the same manner as linear cations. Other binding modes, such as bridging interactions between DNA double helices, may be necessary to induce condensation with dendrimers.[44–48]

Osmotic stress combined with X-ray diffraction allows us to directly measure fundamental molecular scale interactions between DNA helices in ordered assemblies. It was previously shown that both attractive and repulsive forces can be described by exponential functions with fixed ~2.5 Å and ~5 Å decay lengths for DNA condensed by a wide variety of cations including $Co(NH_3)_6^{3+}$, spermidine^{3+}, spermine^{4+}, oligoarginines (Arg_1–Arg_6) and salmon protamine.[24,25] Recently we have learned how to separate and quantitate attractive and repulsive contributions to the overall force.[25,26,28] Herein, we have used low generation PAMAM dendrimers (G0-PAMAM (+4) and G1-PAMAM (+8)) to condense high molecular weight DNA. The force curves of hyperbranched PAMAM molecules are compared to those of linear arginine peptides of the same net charge (tetra-arginine [R_4^{4+}] and octa-arginine [R_8^{8+}]). We have previously shown a length dependent attraction resulting in higher packaging densities with increasing charge for linear cations.[25,28] Our results show that PAMAM–DNA complexes give lower DNA packaging densities with higher dendrimer generation numbers. Fits to the force curve data suggest that this packaging difference arises from both increased repulsions and greatly reduced attractions in PAMAM–DNA compared to the linear cations. We also examined the salt and pH dependence of packaging in dendrimer–DNA complexes compared to the arginine–DNA complexes. The increased pH and salt sensitivities of PAMAM polyplexes are suggestive that different binding modes may be active in the hyperbranched cations.

Experimental methods

Materials

Polyamidoamine (PAMAM) dendrimers (Generation 0 and Generation 1, ethylenediamine core, amine-terminated and 20 wt% solution in methanol) were obtained from Sigma-Aldrich (St Louis, MO). Before use, methanol was removed under reduced pressure at room temperature using a Labconco Centrivap. G0- and G1-PAMAM were subsequently dissolved in deionized water and buffered with acid or base to the desired pH. Tetra-arginine (R_4) and octa-arginine (R_8) peptides were custom synthesized and purified (>98%) by GenScript Corporation. The peptides were neutralized with Tris base and used without further purification. Bioultra grade polyethylene glycol (PEG), with an average molecular weight (MW) of 8000, was purchased from Fluka Chemical Co. All chemicals were used without further purification. Highly polymerized calf-thymus DNA sodium salt (molecular weight ~10–15 million daltons) was purchased from Sigma-Aldrich and subsequently purified by phenol/chloroform extraction to remove excess proteins. High-molecular weight DNA (>5×10^6) was prepared and purified from adult chicken whole blood as described previously.[49] After purification, both chicken blood and calf-thymus DNA were extensively dialyzed against 10 mM Tris–HCl (pH 7.5) and 1 mM EDTA. The successful removal of protein was verified by measuring the ratio of absorbance at 260 nm and 280 nm of DNA solutions (260/280) and it was found to be acceptable with values >1.8.

Sample preparation

For all four cations used in this study (R_4, R_8, G0-PAMAM and G1-PAMAM), DNA spontaneously precipitates and samples for X-ray scattering were prepared in one of two ways. Concentrated polycation solutions were added to 1 mg mL^{-1} chicken erythrocyte DNA or calf-thymus DNA (~250 μg of DNA) in 10 mM Tris–HCl (pH 7.5) in steps of 0.2 mM. Each addition was thoroughly mixed before adding more condensed ions and the process was continued until all DNA was precipitated. Alternatively, condensing cations were added to DNA in a single aliquot to an equivalent final concentration. Typically, the cation to DNA phosphate ratio was 1.5–2 at the end point. The resulting fibrous samples were centrifuged at ~10 000*g* for 10 min and transferred to corresponding PEG–salt solutions and allowed to equilibrate for ~2 weeks. X-ray scattering profiles did not depend on the type of DNA (calf thymus or chicken blood) or the method used to prepare the DNA precipitate. No change in the X-ray scattering pattern was observed after 6 months of storage. PEG osmotic pressures were measured directly using a Wescor Vapro Vapor Pressure Osmometer (model 5660).

For pH dependent studies, samples were prepared with calf thymus DNA dissolved in deionized water. Cations were dissolved in water and buffered to the desired pH (pH range 4–8) with HCl or NaOH. Condensed DNA was then prepared as described above and equilibrated for ~2 weeks in pH appropriate buffer. A second set of pH experiments were performed by condensing calf thymus DNA with cations buffered to pH 5 or pH 8 as described above. After equilibration, these samples were examined by SAXS to determine the interhelical spacing, D_{int}. Subsequently, these condensed DNA samples were then equilibrated for 2 weeks in the opposite pH solution and measured by SAXS to determine the change in D_{int} after changing the pH bath solution.

Critical concentrations

The critical concentration of each condensing cation used for precipitation of DNA from dilute solution was determined as

described by Pelta *et al.*[30] A series of DNA samples was prepared with varied cation concentrations in 10 mM Tris buffer. The DNA concentration was ~15 μM base pairs in a total volume of 1 mL. After incubation at room temperature for ~1 hour, the solution was centrifuged at ~16 000*g* for 10 min and the DNA absorbance at 260 nm of the supernatant was measured. Critical concentrations were observed to decrease approximately by an order of magnitude for each additional charge, as seen by others.[50,51] The cation concentrations used in the bathing PEG–salt solution for the osmotic stress measurements were ~2–10 fold higher than the critical concentration. Over this range, the observed spacing between helices does not depend on the cation concentration.

Osmotic stress

The method for direct force measurements by osmotic stress has been previously described in detail.[19,35] In brief, condensed macromolecular arrays, such as DNA, are equilibrated against a bathing polymer solution of known osmotic pressure. The bathing polymer, typically PEG, is too large to enter the condensed DNA phase, thus applying a direct osmotic pressure on the condensate. Water, salt, and other small solutes are free to exchange between the PEG and condensed DNA phases. After equilibration, the osmotic pressures in both phases are the same. Using small-angle X-ray scattering (SAXS), D_{int} can be determined from the Bragg scattering of X-rays as a function of the applied PEG osmotic pressure to obtain force-*versus*-separation curves.

X-ray scattering

Graded-multilayer focused Cu Kα radiation from a Nonius FR-591 rotating anode fine-focus X-ray generator operating at 45 kV and 20 mA was used for the small-angle X-ray scattering experiments. The primary beam cross-section was limited using a fine rear aperture beam tunnel. Samples were sealed with a bath of equilibrating solution in the sample cell and then mounted into a sample holder at room temperature (25 °C). The flight path between the sample and the detector was filled with helium to minimize background scattering. Diffraction patterns were recorded with a SMART 6000 CCD detector, with phosphor optimized for Cu Kα radiation. The images were analyzed with Fit2d and Origin 8.0 software. The distance from the sample to the detector, calibrated using silver behenate, was found to be ~23.2 cm. In typical scattering experiments, we see not only the Bragg reflection, to determine interaxial DNA–DNA spacings, but also weak higher-order diffraction typical of hexagonal packaging. The Bragg spacing is calculated as $D_{\mathrm{Bragg}} = 2\pi/q_{100}$, where q_{100} is the scattering vector, q, which corresponds to the maximum in the scattering. q is defined as $q = (4\pi/\lambda)\sin\theta$ where 2θ is the scattering angle. For a hexagonal lattice, the Bragg spacing, D_{Bragg}, and the actual distance between helices, D_{int}, are related by $D_{\mathrm{int}} = (2/\sqrt{3})D_{\mathrm{Bragg}}$. For different samples equilibrated under the same PEG–salt conditions, D_{int} values were reproducible to within ~0.1 Å. X-ray scattering patterns were reproducible over at least 6 months of storage and no sample degradation was apparent. Typical exposure times were of the order of 2 minutes.

Force analysis

Many polyvalent cations, including all the linear arginine and PAMAM dendrimers discussed in this work, cause DNA to spontaneously condense *in vitro* resulting in a finite equilibrium separation between the hexagonally packed DNA helices. Thermodynamic forces between polycation condensed DNA helices can be investigated by the osmotic stress technique. Previous results indicated that the DNA–DNA forces can be described by two exponentials at close interaxial spacings, the last 20 Å of surface-to-surface separation.[19,24,25,28] We fit the osmotic pressure Π *versus* spacing D curves to a double exponential equation with variable pre-exponential factors A and R:

$$\Pi(D) = \Pi_R(D) + \Pi_A(D) = R\mathrm{e}^{-2D/\lambda} + A\mathrm{e}^{-D/\lambda} \quad (1)$$

or equivalently

$$\log(\Pi(D)) = \log(R) - \frac{2D}{2.303\lambda} + \log\left(1 + \frac{A}{R}\mathrm{e}^{D/\lambda}\right) \quad (2)$$

with the decay length λ fixed at 5 Å. This form and decay length constraint are the result of experiments combining osmotic stress measurements with single molecule, magnetic tweezer experiments to separate the attractive and repulsive free energies at the equilibrium spacing for several commonly used condensing agents.[24] Eqn (2) with $\lambda = 5.0$ Å gives very good fits for the arginine–DNA complexes previously examined.[25] The results are only slightly dependent on the decay length λ over the range of approximately ±0.5 Å. For cations that induce DNA condensation, such as those used in this study, the coefficients R and A are connected through the equilibrium interaxial spacing D_{eq} because $\Pi(D_{\mathrm{eq}}) = 0$, giving a fitting equation with only a single variable R.

$$\log(\Pi(D)) = \log(R) - \frac{2D}{2.303\lambda} + \log\left(1 - \mathrm{e}^{-(D_{\mathrm{eq}}-D)/\lambda}\right) \quad (3)$$

Assuming hexagonal packing, the repulsive and attractive free energy contributions per DNA base pair can be calculated at a spacing D by integrating $\Pi \mathrm{d}V$ for each exponential from ∞ to D,

$$\frac{\Delta G_R(D)}{kT} = \frac{\sqrt{3}b(\lambda/2)(D + \lambda/2)}{kT}\Pi_R(D) \quad (4)$$

and

$$\frac{\Delta G_A(D)}{kT} = \frac{\sqrt{3}b\lambda(D + \lambda)}{kT}\Pi_A(D) \quad (5)$$

where b is the linear spacing between DNA base pairs, 3.4 Å.

Results

Packing and forces in DNA condensed with G0-PAMAM, G1-PAMAM, tetraarginine (R_4), and octaarginine (R_8)

Fig. 1 shows osmotic stress curves for G0-PAMAM (G0) and G1-PAMAM (G1) condensed DNA. Plotted are log osmotic pressure (Π) values *versus* DNA interaxial spacings D_{int}. These dendrimer–DNA complexes were precipitated at pH 7.5 and buffered with 10 mM Tris (pH 7.5) for all samples. Arrows show the

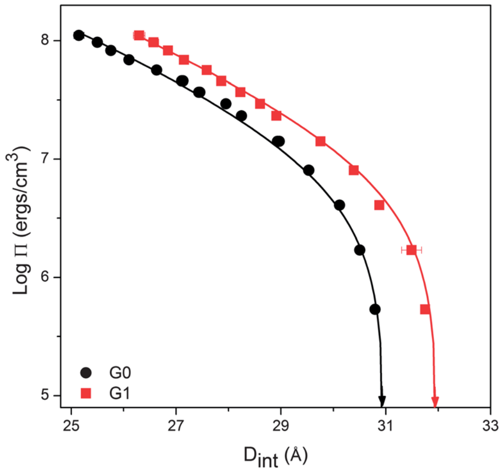

Fig. 1 Osmotic stress force curves are shown for DNA condensed by low generation (G0 and G1) PAMAM. The arrows indicate the equilibrium spacing in the absence of applied PEG osmotic pressure. The solid lines are fits of the data to eqn (3) with $\lambda = 5$ Å.

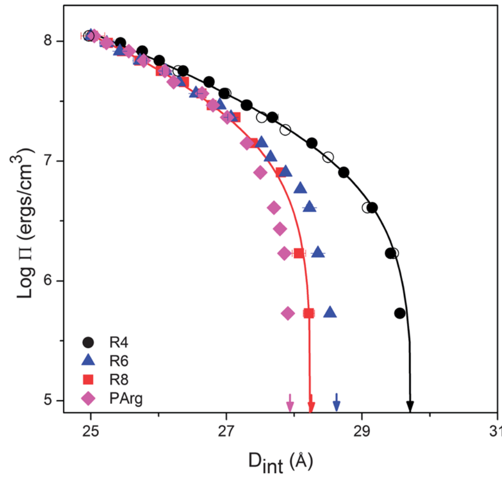

Fig. 2 Osmotic stress force curves are shown for DNA condensed by tetraarginine (R_4) and octaarginine (R_8) peptides. The arrows indicate the equilibrium spacing in the absence of applied PEG osmotic pressure. The solid lines are fits of the data to eqn (3) with $\lambda = 5$ Å. Also shown are tetraarginine (R_4, open circles), hexaarginine (R_6) and polyarginine published previously.[25]

interaxial spacing in the absence of applied osmotic pressure. Solid lines are fits of the data to eqn (3) with the decay length λ fixed at 5.0 Å. Results depend only weakly on the decay length over the range of ∼±0.5 Å. These fits allow us to separate the net force into its attractive and repulsive components. The protonation of G0 and G1 was thoroughly studied previously.[52] At near neutral pH, PAMAM has the complete protonation of the primary amine groups at the dendrimer surface resulting in +4 and +8 surface charges for G0 and G1 respectively. The equilibrium spacing in the absence of applied osmotic pressure increases with increasing PAMAM generation. In addition, the high pressure data do not converge despite the similar chemical moieties on the surface amine groups as we have seen with other homologous cations.

Fig. 2 shows the osmotic stress curves for tetraarginine (R_4) and octaarginine (R_8) condensed DNA at pH 7.5. These linear polycations are the charge equivalent arginine peptides to G0 and G1. Arrows show the interaxial spacing in the absence of applied osmotic pressure. Solid lines are fits to eqn (3) with λ fixed at 5.0 Å. As reported previously, despite starting at very different equilibrium spacings without applied osmotic pressure, the high pressure data converge to the same high pressure limit. To emphasize this convergence at high pressure, we have also plotted previously published data for R_4, R_6 and polyarginine (MW ∼ 35.5 kDa, PArg).[25] Increasing the number of arginines in this linear series results primarily in an increase of the magnitude of the 5.0 Å attractive decay length. At the highest osmotic pressures, the 2.5 Å repulsive decay length dominates and is only slightly dependent on the number of arginines. We previously showed that the attractive free energy for linear arginine has a $\sim 1/N$ dependence for the arginine series from R_2 through R_6 and poly(Arg).[25] The R_4 and R_8 data shown in Fig. 2 are consistent with these previous observations.

Fig. 3 shows typical X-ray scattering intensity profiles for all four cation polyplexes in Tris buffer (pH 7.5) without additional salt. Without applied osmotic pressure, the equilibrium interaxial spacings, $D_{\rm int}$, between helices in G0-DNA and G1-DNA complexes are 31.0 Å and 32.0 Å (±0.1 Å) respectively. R_4–DNA and R_8–DNA have $D_{\rm int}$ of 29.8 Å and 28.3 Å (±0.1 Å), respectively. The sharp peak for all complexes is the helix–helix Bragg reflection. The peaks at larger Q are consistent with 101 and 110 reflections for a hexagonal lattice. These higher order reflections are indicated by arrows in Fig. 3. The presence of

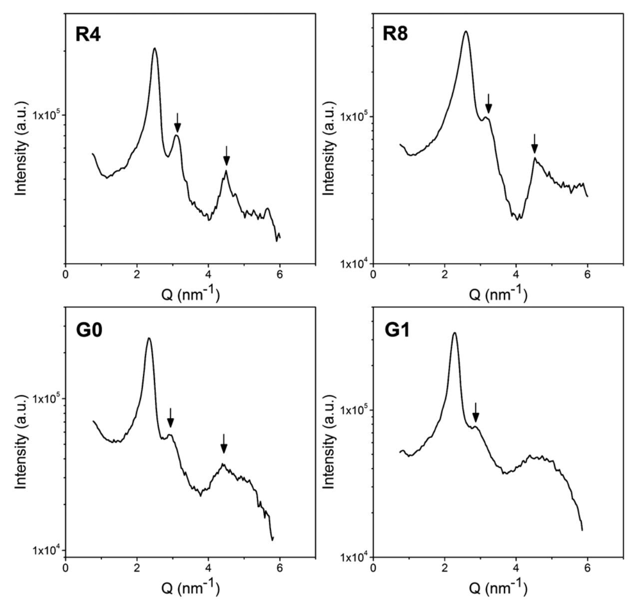

Fig. 3 Small-angle X-ray scattering (SAXS) profiles of DNA assemblies condensed by R_4, R_8, G0-PAMAM, and G1-PAMAM in 10 mM Tris, pH 7.5. Higher order reflections, indicated by arrows, are consistent with (101) and (110) reflections of a hexagonal lattice. These reflections are clearly evident in R_4 and R_8 condensed DNA. G0-PAMAM also shows these peaks but they are reduced. G1-PAMAM shows further reduction of the (101) reflection and no evidence of the (110) reflection.

these higher order reflections has been previously assigned as evidence of the binding of cations in grooves.[39] The amplitude of these higher order reflections is much larger for the linear arginine condensed polyplexes than the hyperbranched PAMAM dendriplexes. We also note that while the PAMAM dendriplexes do maintain a 101 reflection, the 110 reflection ($Q \sim 4.5$–5 nm^{-1}) is very weak in G0-DNA and non-existent in the larger G1-DNA samples. The equilibrium spacings, osmotic pressure contributions at 25 Å, Π_R (25 Å) and Π_A (25 Å), and the free energy contributions ΔG_R (25 Å) and ΔG_A (25 Å) for the PAMAM and arginine cations are given in Table 1. The free energy contributions show that PAMAM dendrimers have comparable repulsive contributions to their arginine equivalents. G1 has increased repulsions compared to R_8. Significantly, the attractive free energy contributions are greatly reduced for both G0 and G1 when compared to the linear R_4 and R_8 systems.

Role of pH on equilibrium spacings

To investigate the role of pH on the resulting equilibrium interaxial spacings, two sets of experiments were performed. In the first set of experiments, condensing agents were buffered to different pH values (pH 4–8) from stock solutions with HCl or NaOH. Calf thymus DNA in distilled water was then precipitated with the pH buffered cations as described in the Methods section. Samples were equilibrated for two weeks in fresh pH buffered aqueous solutions with a slight excess of polycation to maintain the cation concentration above the critical concentration. It is known that at lower pH, the tertiary amines of PAMAM can become protonated thus shifting the charge density higher. Such pH effects are not expected in arginine peptides over most pH values because the pK_a value of the guanidyl group in arginine is ~12.5. Fig. 4 shows the results of the equilibrium spacing as a function of the pH at condensation for R_4, R_8 and G0, G1 PAMAM condensed DNA. Here, we plot the change in interhelical spacing ΔD_{int} relative to precipitation in 10 mM Tris, pH 7.5 ($\Delta D_{int} = \Delta D_{int,pH} - \Delta D_{int,pH\ 7.5}$). As pH decreases, we see decreasing equilibrium spacings for all four cationic species. As expected R_4 and R_8 show only slight changes (~0.3–0.5 Å) in equilibrium spacings over the pH range studied. PAMAM complexes show significantly larger pH dependence. G0 changes ~1.2 Å between pH 4 and 8 while D_{int} changed ~2.9 Å for G1 over the same pH range. At pH 4, the DNA interhelical spacing is now smaller for G1 than for G0, the opposite of pH 8. These differences highlight the pH sensitivity

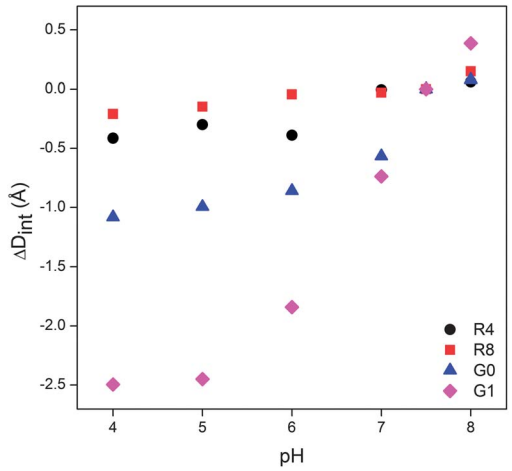

Fig. 4 Effect of changing pH at condensation. The changes in interhelical spacings ($\Delta D_{int} = D_{int,pH} - D_{int,Tris}$) are shown as a function of the solution pH at condensation. All cations are normalized relative to condensation at 10 mM Tris, pH 7.5.

of the resulting packaging densities in PAMAM dendriplex complexes.

In the second set of experiments, PAMAM–DNA was condensed at pH 5 and pH 8. Samples were equilibrated for one week and measured by SAXS to determine the interaxial equilibrium spacing, D_{int}. The measured equilibrium spacings were consistent with the pH results described in Fig. 4. The change in equilibrium spacing between condensation at pH 5 and pH 8 was ~1.1 Å and 2.8 Å for G0 and G1 respectively. The condensed PAMAM–DNA condensates were then switched from pH 5 to pH 8, re-equilibrated, and examined by X-ray diffraction to determine the effect of changing the buffer pH on the condensed PAMAM–DNA fibers. Results are shown in Table 2. D_{int} values were reproducible to within ~0.1 Å. Although large changes in D_{int} were observed upon changing the pH at condensation for PAMAM–DNA, once condensed the effect of pH change on D_{int} was significantly smaller. A change in pH buffer solutions was evidenced most clearly in G1. Condensing DNA with G1 at pH 5 and then subsequently equilibrating at pH 8 was observed to increase its interaxial spacing. However, the observed increase of 1.4 Å is only about half of the observed D_{int} change measured when DNA was condensed by G1 at pH 5 and pH 8. Condensing at pH 8 and then equilibrating to pH 5 resulted in a shift of the D_{int} for G1-DNA of ~0.7 Å from 32.3 Å to 31.7 Å. DNA condensed by G0 displayed a similar behaviour. Both pH buffer changes on

Table 1 The equilibrium interhelical spacings (±0.1 Å) from direct X-ray measurements and repulsive and attractive force component contributions to osmotic pressures (±5%) and free energies (±5%) at 25 Å calculated from fits to force curves are shown for DNA condensed by the four cations used in this study

Cation	D_{eq} (Å)	Π_R (25 Å) (10^8 erg cm^{-3})	Π_A (25 Å) (10^8 erg cm^{-3})	ΔG_R (25 Å) kT per base pair	$-\Delta G_A$ (25 Å) kT per base pair
R_4	29.8	1.91	0.74	1.89	1.59
R_8	28.3	2.35	1.23	2.32	2.64
G0-PAMAM	31.0	1.80	0.55	1.79	1.18
G1-PAMAM	32.0	2.67	0.66	2.64	1.43

Table 2 Effect of changing buffer pH after condensation for low generation PAMAM–DNA complexes. Samples were condensed at pH 5 or pH 8 and allowed to equilibrate for two weeks and measured by X-ray diffraction to determine interaxial DNA spacings. Samples were then placed in the opposite pH buffer, allowed to re-equilibrate for two weeks and reexamined by scattering

	G0-PAMAM		G1-PAMAM	
	Condensed at pH 5	Condensed at pH 8	Condensed at pH 5	Condensed at pH 8
D_{int}, buffer pH 5	30.0 Å	30.9 Å	29.5 Å	31.7 Å
D_{int}, buffer pH 8	30.2 Å	31.0 Å	30.9 Å	32.4 Å
ΔD_{int} buffer change	0.2 Å	~0.07 Å	1.4 Å	0.7 Å
ΔD_{int} pH at condensation	1.1 Å		2.8 Å	

condensed PAMAM–DNA complexes were considerably smaller than the ΔD_{int} observed from condensing DNA at different pHs. When returned to their initial pH conditions, the measured equilibrium spacings for both G0 and G1 condensed DNA were within 0.2 Å of their original values.

Salt dependence of R_4, R_8, G0-PAMAM and G1-PAMAM

Fig. 5 shows the change in interhelical spacing as the NaCl salt concentration is increased. In all the curves, the slight excess polycation concentration in the bathing solution was maintained in 10 mM Tris, pH 7.5. As phase transitions may occur with increasing salt, we plot simply the salt dependence of the Bragg reflection $D_{Bragg} = 2\pi/q_{100}$. Fig. 5A plots the Bragg spacing dependence for all four cation condensed DNA systems as a function of added NaCl salt concentration. Fig. 5B shows the relative change in the Bragg spacing compared to no excess salt ($D_{Bragg,salt} - D_{Bragg,Tris}$) for each cation–DNA complex. All four samples show swelling of the DNA array with increasing added NaCl salt concentration; however the swelling behaviour is highly dependent on the condensing cation. With increasing salt, the DNA–cation fiber swells reaching a salt concentration where no Bragg scattering is observed within the sample. At even higher NaCl salt concentrations, the samples completely dissolve. For the linear arginine cations, increasing the cation charge from R_4 to R_8 resulted in a significantly more salt stable complex. For R_4–DNA, a steady increase in D_{Bragg} is observed for 0 to 150 mM added NaCl salt. Bragg scattering is no longer observed at 200 mM salt. The larger R_8 shows the least dependence of D_{Bragg} on NaCl salt concentration. For R_8–DNA, stable Bragg reflections are observed for 700 mM NaCl. By 800 mM NaCl, Bragg reflections in R_8–DNA are lost. This behaviour is in stark contrast to the PAMAM dendriplexes. For NaCl salt concentrations less than ~0.1 M, the changes in spacing for $G0^{+4}$ and R_4^{4+} are quite similar. By 125 mM NaCl, G0-DNA swells significantly more than R_4–DNA to $D_{Bragg} \sim 30.0$ Å ($D_{int} \sim 34.7$ Å). Bragg scattering is lost for G0-DNA by 150 mM NaCl. More pronounced is the difference between the octa-valent R_8 and G1 condensed DNA systems. G1-DNA swells to $D_{Bragg} \sim 33.2$ Å by 250 mM NaCl and all Bragg scattering is lost by 275 mM NaCl compared to 800 mM for linear R_8.

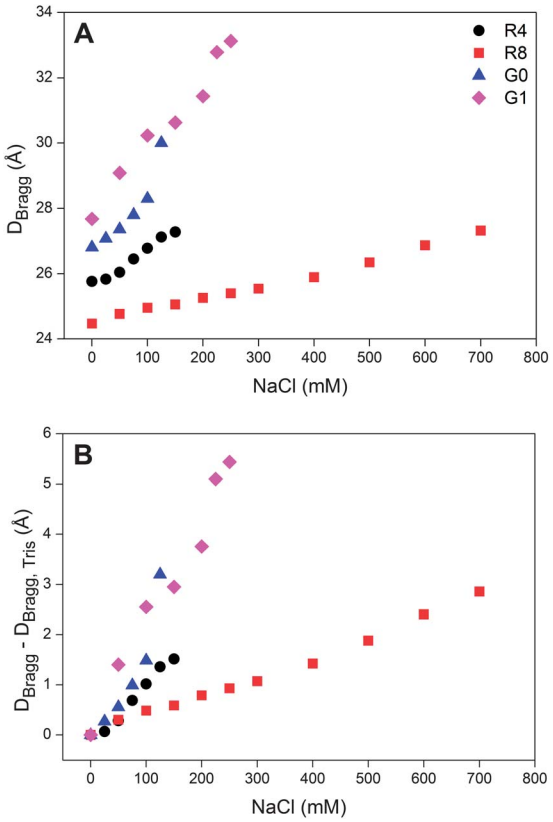

Fig. 5 (A) Bragg spacing dependence ($D_{Bragg} = 2\pi/q_{100}$) *vs.* added NaCl concentration for R_4, R_8, G0 and G1-DNA systems. (B) The change in the Bragg spacing relative to D_{Bragg} in 10 mM Tris without added salt. The equilibrium solutions show no scattering at the next higher salt concentration in each series.

Fig. 6 shows typical scattering profiles with Bragg reflections for all four cation–DNA systems at low and high salt concentrations. The higher order reflections gradually disappear for all systems with increasing salt concentration. For R_4 and R_8, the scattering profiles show predominantly a simple shifting of the sharp Bragg reflection to lower q (*i.e.* larger DNA–DNA spacings). The PAMAM–DNA samples however display a significant peak broadening with increased salt concentration. For PAMAM condensed DNA, the Bragg peaks at high salt concentrations broaden approximately two times the width of the sharp low salt reflections. Such peak broadening is consistent with a columnar to cholesteric transition.

Discussion

Much previous work has been done to study *in vitro* condensation of DNA by a variety of multivalent ions. Typically cations of net charge greater than +3 are capable of condensing DNA into hexagonal arrays. Depending on the cation used to condense, the DNA helices within these arrays do not touch but are separated by ~7–15 Å of water. This water separation represents a delicate balance of the attractive and repulsive forces within these soft matter phases. To account for the magnitude of the attractions driving DNA condensation, most

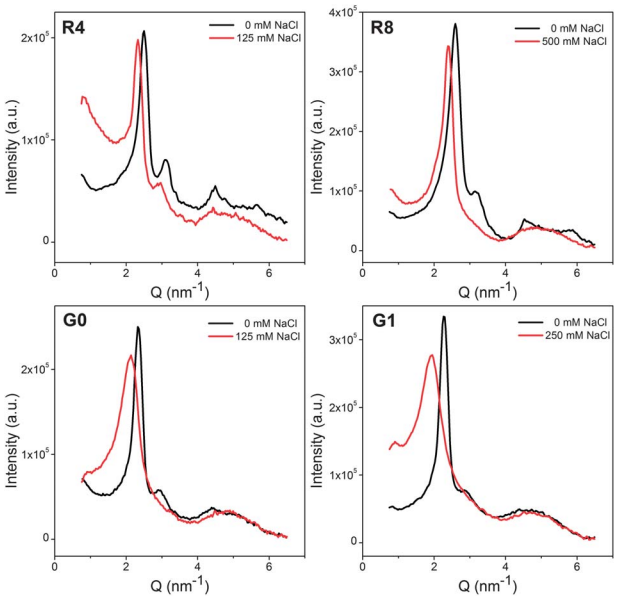

Fig. 6 Scattering profiles for DNA assemblies condensed by R_4, R_8, G0-PAMAM, and G1-PAMAM at 10 mM Tris, pH 7.5 and with higher added NaCl concentration. All samples have a clear shift to lower Q (or equivalently larger D_{Bragg}) with added salt. The arginine–DNA samples maintain a sharp Bragg peak at high and low salt concentrations while the G0- and G1-PAMAM show significant peak broadening with added salt.

current theoretical models require a correlation of charge or water structuring. Typically, this correlation is accomplished by assuming cation binding to the major or minor grooves of DNA. Such correlations thus allow for the bound positive charges on one DNA to correlate and interact with the negative phosphate backbone of an apposing DNA helix. Prior experimental results have also suggested binding of linear cations within DNA grooves for a variety of linear cationic systems.[39–43] For dendrimers or spherical polycations, other binding modes such as cation bridging between DNA double helices have been proposed.[44–48]

Dendrimers are well known to be able to condense and protect nucleic acids from degradation by nucleases. The size and hyperbranched nature of dendrimers, however, suggest that correlation of charge (or water structuring) within grooves is unlikely. Most of the structural studies to date have observed hexagonal arrangement of the DNA helices when complexed with low generation PAMAM dendrimers (<G4) similar to linear cations. The surface charges of G0 and G1 at neutral pH are +4 and +8, respectively, and they have theoretical diameters of 15 and 22 Å. G0 and G1 condensed DNA at pH 7.5 have D_{int} of ~31 and 32 Å. B-DNA has a diameter of 20 Å leaving 11 and 12 Å of water separating the DNA helices in these PAMAM condensed DNA phases. The resulting spacings are smaller than the theoretical dendrimer diameters. While high generation dendrimers are predicted to be spherical in shape, low generation dendrimers are believed to be more of a disc-like shape which may help the low generation dendrimers to fit within the DNA arrays.[18] It is also important to note that B-DNA has major groove dimensions of approximately 8.5 Å deep and 11.7 Å wide. Linear multi-valent cations such as metal ions, alkyl amines, and arginine and lysine peptides are able to fit comfortably into grooves. However, even low generation dendrimer molecules are comparable in size to the major groove dimensions, thus presumably are unable to access the DNA grooves. If unable to correlate within DNA grooves, other modes of binding, such as charge bridging across two DNA molecules, may dominate the dendrimer–DNA interactions.

To investigate the role of cation chain architecture, we have compared osmotic stress force curves of G0- and G1-PAMAM to comparably charged tetra- and octa-arginine (R_4/R_8) linear peptides. Despite its simplicity the double exponential form of eqn (2) and (3) with fixed 2.5 and 5.0 Å decay lengths gives good fits to all the force data shown in Fig. 1 and 2. The equilibrium distances between DNA helixes are determined by the balance of attractions and repulsions within the cation–DNA system and are cation specific. We previously showed using linear homopeptides that the repulsive force is only weakly dependent on the peptide length (or equivalent charge) while the attractive force increases with the number of arginine repeats and dominates the interactions at charges ≥+3. Combined, these attractions and repulsions result in the interaxial spacing between DNA helices decreasing with increasing number of repeats in a linear homopeptide such as the arginine data shown in Fig. 2. The attractive free energies measured for R_4 and R_8 in this paper are consistent with the ~1/N dependence for the arginine series previously measured.[25] We argue that the 1/N dependence is a result of translational entropy of the bound cation. In other words, there is less loss of entropy to correlate one +4 counterion than four +1 ions. We have shown that oligolysines and simple alkyl amines (putrescine^{2+}, spermidine^{3+}, and spermine^{4+}) show a similar 1/N behaviour.[25,28]

DNA condensed by G0- and G1-PAMAM show completely different behaviour in the force curves. While all four systems are well described by the double exponential formalism given in eqn (3), the attraction and repulsive forces show different trends for branched dendrimers compared to their charge equivalent linear arginines. Not only does the equilibrium interhelical spacing increase in Fig. 1 with increasing charge for PAMAM but the high pressure data do not converge despite the chemical similarity in the terminal primary amines for both PAMAM species. The results of the force curve fits in Table 1 indicate that the hyperbranched nature of the dendrimer results in slightly higher repulsions and significantly reduced attractions when compared to the linear cations. Increasing the linear arginine peptide from R_4 to R_8 results in a 66% increased attraction which overcomes the ~23% increase in repulsions. These forces result in tighter DNA packaging for R_8 compared to R_4. In comparison, comparing G0 and G1 we see that the repulsions are increased ~47% while the increased attraction of the octavalent G1 is only ~21% greater than the tetravalent G0. The decrease in the long range attractive force amplitude is significantly greater than the increase in the short range repulsive force. This decreased attraction is consistent with the notion that cationic dendrimers are unable to correlate their charges with the phosphates of adjoining DNA in the same manner as linear cations. Indeed the attractions measured for

G1 are still less than for R_4. The corresponding additional repulsive force observed for PAMAM could be due to the compressibility of the branched dendrimer, but warrants further study.

The pH and salt dependencies of the DNA–DNA spacings at equilibrium for the cation–DNA complexes used in this study were determined by SAXS. PAMAM dendrimers have tertiary amine groups at each branching point and primary amines at each terminal end. The protonation level of the PAMAM can therefore be altered significantly by changing the solution pH. At physiological pH, the primary amines are protonated while at low pH, the tertiary amines in PAMAM dendrimers can carry charge. G0 has 4 primary and 2 tertiary amines. G1 has 8 primary and 6 tertiary amines. The charges on arginine peptides are relatively pH insensitive as the pK_a value of the guanidyl group of arginine is ∼12.5. Fig. 4 shows the effect of changing the pH at which condensation occurs for the arginine and PAMAM condensed DNA systems from pH 4 to 8. Prior work showed DNA condensation occurs when over 90% of its charge is neutralized by counterions.[29] The increasing protonation state of PAMAM at lower pH would require less mass of dendrimer to neutralize the charge of the DNA phosphates. Less dendrimer within the condensate would presumably lead to more close packing of the DNA helices as is observed. The pH effect is as follows: tighter packaging of the DNA is observed for both G0 and G1 at low pH; however G1 showed significantly larger differences in equilibrium spacing than G0 over the same pH range. The arginine peptides (R_4 and R_8) also show a slight decrease in D_{int} at low pH. This is perhaps due to some protonation of the C-terminal carboxyl of these peptides ultimately increasing their overall net charge. If the C-terminal carboxyl of the arginines is partially protonated, we would expect tighter packaging of the DNA due to the previously discussed $1/N$ dependence of the attractions. This $1/N$ dependence is also consistent with the observation that the change in the interaxial spacing (ΔD_{int}) is larger for R_4 than for R_8 as a larger relative change in attractive free energy would be expected upon moving from +4 to +5 than from +8 to +9.

Once condensed, changing the buffer pH does induce a shift in the equilibrium DNA spacing in the direction anticipated from Fig. 4. However, the magnitude of the spacing shift was significantly less as shown in Table 2. These results suggest that once bound, the pK_as of the tertiary amines in PAMAM are shifted and their ability to protonate or deprotonate is different than PAMAM in free solution. Interestingly, the ability to respond to pH is asymmetric. Both PAMAM–DNA complexes undergo a larger change in equilibrium spacing when condensed at low pH and then re-equilibrated at high pH than *vice versa*. When returned to their original pH, the D_{int} spacings did return to within ±0.2 Å of their original spacing. One explanation for this phenomenon would be that the exchange of PAMAM from the condensate and bulk solution may be slow and meta-stable.

Lastly, we examined the effect of NaCl salt on our PAMAM and arginine condensed DNA assemblies. We have previously studied the salt dependence of protamine–DNA complexes showing that salt has a two-fold action: both anion binding to protamine and cation competition with protamine for DNA binding.[27] An increasing ionic strength would also screen possible electrostatic attractive forces. For linear cations, larger spacings at high salt concentrations suggest a decrease in attractive free energy due to a weakened correlation of the cation, or a decreased charge of the bound polycation with anion binding or increased shielding of charges on adjacent helices. If bridging or other binding modes are active in dendrimer–DNA complexes, it is reasonable to assume that the salt sensitivities would be different than the linear cation–DNA complexes. As shown in Fig. 5, swelling occurs for all four systems. Both PAMAM systems are observed to swell to significantly larger spacings and lose Bragg reflections at lower salt concentrations than their equivalently charged linear arginine peptides. The salt concentration at which Bragg scattering was no longer observed was highly charge dependent for linear arginine shifting from ∼200 mM to ∼800 mM for R_4 and R_8 respectively. Over these NaCl salt concentrations, D_{Bragg} swelled approximately 1.5 Å and 3 Å in total for R_4 and R_8 respectively. Interestingly, both arginines reached a $D_{Bragg} \sim 31.5$ Å at the highest salt concentrations. In contrast, the PAMAM complexes swell to much larger Bragg spacings increasing ∼3 and 6 Å for G0 and G1 respectively with increased NaCl concentration. Despite the doubling of the charge in G1, the slope of the Bragg spacing with increasing salt was nearly identical to G0. Unlike arginine, the critical salt concentration at which Bragg spacing was lost for PAMAM only mildly shifted from 150 mM to ∼275 mM with increasing generation number. Using protamine–DNA arrays, we previously showed that salt sensitivities were very dependent on salt species.[27] Specifically, we showed that attractive forces were weakened by a combination of anion binding and cation screening (competition). If anion binding dominates, such as for chaotropic anions, we observe strong dependence of spacings on salt concentration. If cation competition for binding dominates, then weak dependence of DNA spacings was observed. It is also true that with anion binding ($NaSO_4$ or NaSCN), protamine–DNA spacings got much larger before the pellet dissolved than for cation competition (NaF or NaOAc) as with R_8 *vs.* G1. Here, however, these differences are likely arising from different binding modes for branched dendrimers and linear arginines.

In addition, while no significant peak broadening was detected for the arginine–DNA systems, PAMAM–DNA displayed significant peak broadening at high salt concentrations suggestive of a phase transition from a hexagonal packing of DNA to a more loosely ordered liquid crystalline phase. Previously, we observed in high molecular weight polyarginine–DNA complexes that such phase transitions occurred over a narrow range of salt concentrations.[23] For such short polycations as the arginines used in this study, this range may be even narrower and was therefore not observed. PAMAM complexes appear to have this phase transition occur over a broader range of salt concentrations and thus are easily observed. Peak widths are indicative of the average in-plane domain sizes with sharper peaks suggestive of larger domain sizes. Such peak broadening is consistent with a phase transition at high salt concentrations from a columnar hexagonal phase to a more loosely ordered

cholesteric liquid-crystal phase. Similar phase transitions were previously observed for larger generation PAMAM–DNA complexes.[7,17]

Conclusions

The current study represents an investigation of the influence of cation topography on the resulting structure and forces within DNA assemblies condensed by low generation PAMAM dendrimers. In order to compact DNA, linear cations are believed to bind in DNA grooves and to interact with the phosphate backbone of apposing helices. We previously showed a length dependent attraction resulting in higher packaging densities with increasing charge for linear cations. Dendrimers, such as PAMAM, presumably are too large in size and hyperbranched and thus are unable to bind to DNA and correlate their charges in the same manner as linear cations. Using osmotic stress, we have directly probed the DNA–DNA intermolecular forces in PAMAM dendrimer condensed DNA assemblies and compared them to DNA condensed by comparably charged linear arginine peptides. All complexes studied were found to self-assemble into columnar hexagonal phases. The resulting osmotic stress force curves for all four systems are well described by a double-exponential fit with fixed 2.5 and 5.0 Å decay lengths. Separation of the attractive and repulsive contributions to the free energy tells us much about the cation-dependent thermodynamic forces in these systems. We show that PAMAM–DNA assemblies display significantly different physical behaviour than linear cation–DNA assemblies. DNA assemblies condensed with the branched PAMAM dendrimers result in increased repulsions and significantly weakened attractions compared to comparably charged linear arginines. These changes in the intermolecular forces result in higher dendrimer generation giving lower DNA packaging densities, the opposite behaviour of linear cations. In addition, significant differences in pH and salt dependencies in the PAMAM dendriplexes are observed. Our data are highly suggestive that other binding modes, such as bridging interactions between DNA double helices, may be necessary to induce condensation with dendrimers. These studies begin to elucidate the role of cation topography in DNA condensation.

Acknowledgements

This research was supported by start-up funds from the University of Kentucky. We would also like to thank Drs Donald Rau and Rudi Podgornik for useful discussions.

References

1 A. U. Bielinska, C. L. Chen, J. Johnson and J. R. Baker, *Bioconjugate Chem.*, 1999, **10**, 843–850.
2 J. D. Eichman, A. U. Bielinska, J. F. Kukowska-Latallo and J. R. Baker, Jr, *Pharm. Sci. Technol. Today*, 2000, **3**, 232–245.
3 D. W. Pack, A. S. Hoffman, S. Pun and P. S. Stayton, *Nat. Rev. Drug Discovery*, 2005, **4**, 581–593.
4 C. Dufès, I. F. Uchegbu and A. G. Schätzlein, *Adv. Drug Delivery Rev.*, 2005, **57**, 2177–2202.
5 K. K. Kunze and R. R. Netz, *Phys. Rev. Lett.*, 2000, **85**, 4389–4392.
6 M. Jonsson and P. Linse, *J. Chem. Phys.*, 2001, **115**, 10975–10985.
7 H. M. Evans, A. Ahmad, K. Ewert, T. Pfohl, A. Martin-Herranz, R. F. Bruinsma and C. R. Safinya, *Phys. Rev. Lett.*, 2003, **91**, 075501.
8 Y. C. Liu, H. L. Chen, C. J. Su, H. K. Lin, W. L. Liu and U. S. Jeng, *Macromolecules*, 2005, **38**, 9434–9440.
9 R. Dootz, A. Otten, S. Koster, B. Struth and T. Pfohl, *J. Phys.: Condens. Matter*, 2006, **18**, S639–S652.
10 T. Pfohl, A. Otten, S. Koester, R. Dootz, B. Struth and H. M. Evans, *Biomacromolecules*, 2007, **8**, 2167–2172.
11 M.-L. Ainalem and T. Nylander, *Soft Matter*, 2011, **7**, 4577–4594.
12 A. M. Carnerup, M.-L. Ainalem, V. Alfredsson and T. Nylander, *Soft Matter*, 2011, **7**, 760–768.
13 C.-Y. Chen, C.-J. Su, S.-F. Peng, H.-L. Chen and H.-W. Sung, *Soft Matter*, 2011, **7**, 61–63.
14 R. Dootz, A. C. Toma and T. Pfohl, *Soft Matter*, 2011, **7**, 8343–8351.
15 E. Froehlich, J. S. Mandeville, C. M. Weinert, L. Kreplak and H. A. Tajmir-Riahi, *Biomacromolecules*, 2011, **12**, 511–517.
16 F. Ritort, S. Mihardja, S. B. Smith and C. Bustamante, *Phys. Rev. Lett.*, 2006, **96**, 118301.
17 K. Fant, E. K. Esbjorner, P. Lincoln and B. Norden, *Biochemistry*, 2008, **47**, 1732–1740.
18 I. Lee, B. D. Athey, A. W. Wetzel, W. Meixner and J. R. Baker, *Macromolecules*, 2002, **35**, 4510–4520.
19 D. C. Rau and V. A. Parsegian, *Biophys. J.*, 1992, **61**, 246–259.
20 E. Raspaud, M. Olvera de la Cruz, J. L. Sikorav and F. Livolant, *Biophys. J.*, 1998, **74**, 381–393.
21 C. C. Conwell, I. D. Vilfan and N. V. Hud, *Proc. Natl. Acad. Sci. U. S. A.*, 2003, **100**, 9296–9301.
22 J. Yang and D. C. Rau, *Biophys. J.*, 2005, **89**, 1932–1940.
23 J. DeRouchey, R. R. Netz and J. O. Radler, *Eur. Phys. J. E: Soft Matter Biol. Phys.*, 2005, **16**, 17–28.
24 B. A. Todd, V. A. Parsegian, A. Shirahata, T. J. Thomas and D. C. Rau, *Biophys. J.*, 2008, **94**, 4775–4782.
25 J. E. DeRouchey, V. A. Parsegian and D. C. Rau, *Biophys. J.*, 2010, **99**, 2608–2615.
26 J. E. DeRouchey and D. C. Rau, *J. Biol. Chem.*, 2011, **286**, 41985–41992.
27 J. E. DeRouchey and D. C. Rau, *J. Phys. Chem. B*, 2011, **115**, 11888–11894.
28 J. E. DeRouchey, B. Hoover and D. C. Rau, *Biochemistry*, 2013, **52**, 3000–3009.
29 R. W. Wilson and V. A. Bloomfield, *Biochemistry*, 1979, **18**, 2192–2196.
30 J. Pelta, F. Livolant and J. L. Sikorav, *J. Biol. Chem.*, 1996, **271**, 5656–5662.
31 W. M. Gelbart, R. F. Bruinsma, P. A. Pincus and V. A. Parsegian, *Phys. Today*, 2000, **53**, 38–44.
32 I. Rouzina and V. A. Bloomfield, *J. Phys. Chem.*, 1996, **100**, 9977–9989.
33 B. Y. Ha and A. J. Liu, *Phys. Rev. Lett.*, 1997, **79**, 1289–1292.
34 B. I. Shklovskii, *Phys. Rev. Lett.*, 1999, **82**, 3268–3271.

35 V. A. Parsegian, R. P. Rand, N. L. Fuller and D. C. Rau, *Methods Enzymol.*, 1986, **127**, 400–416.

36 A. A. Kornyshev and S. Leikin, *Proc. Natl. Acad. Sci. U. S. A.*, 1998, **95**, 13579–13584.

37 A. A. Kornyshev and S. Leikin, *Phys. Rev. Lett.*, 1999, **82**, 4138–4141.

38 A. A. Kornyshev, D. J. Lee, S. Leikin and A. Wynveen, *Rev. Mod. Phys.*, 2007, **79**, 943–996.

39 I. Fita, J. L. Campos, L. C. Puigjaner and J. A. Subirana, *J. Mol. Biol.*, 1983, **167**, 157–177.

40 B. G. Feuerstein, N. Pattabiraman and L. J. Marton, *Nucleic Acids Res.*, 1990, **18**, 1271–1282.

41 N. V. Hud, F. P. Milanovich and R. Balhorn, *Biochemistry*, 1994, **33**, 7528–7535.

42 J. Ruiz-Chica, M. A. Medina, F. Sanchez-Jimenez and F. J. Ramirez, *Biophys. J.*, 2001, **80**, 443–454.

43 A. A. Ouameur and H. A. Tajmir-Riahi, *J. Biol. Chem.*, 2004, **279**, 42041–42054.

44 H. Boroudjerdi and R. R. Netz, *Europhys. Lett.*, 2003, **64**, 413.

45 R. R. Netz and J.-F. Joanny, *Macromolecules*, 1999, **32**, 9013–9025.

46 M. Mills, B. Orr, M. M. B. Holl and I. Andricioaei, *Biophys. J.*, 2010, **98**, 834–842.

47 M. Mills, B. G. Orr, M. M. B. Holl and I. Andricioaei, *J. Phys. Chem. B*, 2013, **117**, 973–981.

48 R. Podgornik and M. Licer, *Curr. Opin. Colloid Interface Sci.*, 2006, **11**, 273–279.

49 J. D. McGhee, W. I. Wood, M. Dolan, J. D. Engel and G. Felsenfeld, *Cell*, 1981, **27**, 45–55.

50 N. Korolev, N. V. Berezhnoy, K. D. Eom, J. P. Tam and L. Nordenskiold, *Nucleic Acids Res.*, 2009, **37**, 7137–7150.

51 I. Nayvelt, T. Thomas and T. J. Thomas, *Biomacromolecules*, 2007, **8**, 477–484.

52 D. Cakara, J. Kleimann and M. Borkovec, *Macromolecules*, 2003, **36**, 4201–4207.